

VIN-NBV: A View Introspection Network for Next-Best-View Selection for Resource-Efficient 3D Reconstruction

Noah Frahm
UNC Chapel Hill
nofrahm@cs.unc.edu

Dongxu Zhao*
UNC Chapel Hill
dongxuz1@cs.unc.edu

Andrea Dunn Beltran*
UNC Chapel Hill
asdunnbe@cs.unc.edu

Ron Alterovitz
UNC Chapel Hill
ron@cs.unc.edu

Jan-Michael Frahm
UNC Chapel Hill
jmf@cs.unc.edu

Junier Oliva
UNC Chapel Hill
joliva@cs.unc.edu

Roni Sengupta
UNC Chapel Hill
ronisen@cs.unc.edu

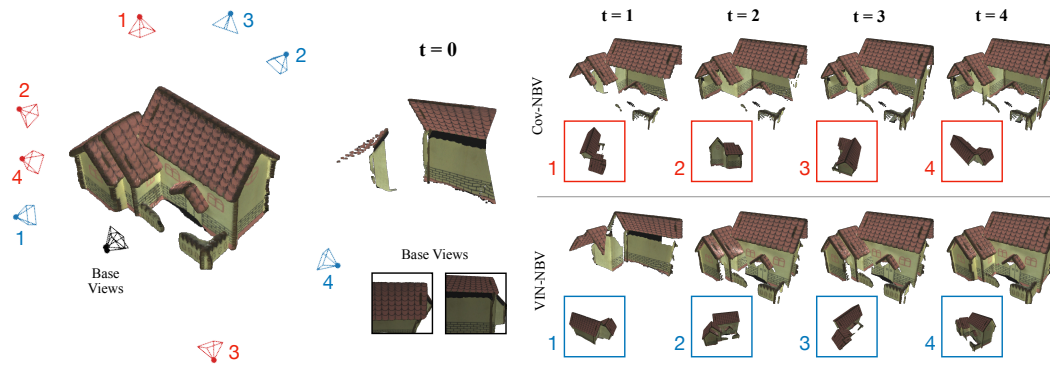


Figure 1: We present VIN-NBV, an NBV policy that selects Next Best Views by maximizing predicted reconstruction quality with limited resources. VIN-NBV (blue) outperforms coverage-based Cov-NBV (red), achieving higher reconstruction accuracy with fewer acquisitions.

Abstract: Next Best View (NBV) algorithms aim to acquire an optimal set of images using minimal resources, time, or number of captures to enable efficient 3D reconstruction of a scene. Existing approaches often rely on prior scene knowledge or additional image captures and often develop policies that maximize coverage. Yet, for many real scenes with complex geometry and self-occlusions, coverage maximization does not lead to better reconstruction quality directly. In this paper, we propose the View Introspection Network (VIN), which is trained to predict the reconstruction quality improvement of views directly, and the VIN-NBV policy. A greedy sequential sampling-based policy, where at each acquisition step, we sample multiple query views and choose the one with the highest VIN predicted improvement score. We design the VIN to perform 3D-aware featurization of the reconstruction built from prior acquisitions, and for each query view create a feature that can be decoded into an improvement score. We then train the VIN using imitation learning to predict the reconstruction improvement score. We show that VIN-NBV improves reconstruction quality by $\sim 30\%$ over a coverage maximization baseline when operating with constraints on the number of acquisitions or the time in motion.

Keywords: 3D Reconstruction, Next Best View, Imitation Learning

*Equal contribution.

†Project page: [Here](#)

1 Introduction

Acquiring 3D knowledge of an environment is often a crucial step for many robotics applications; e.g., a drone surveying a disaster zone to gather information for assisting search and rescue efforts, or autonomous robots monitoring large construction and agricultural sites to gather necessary information. Real-world environments contain diverse objects of varying sizes, occluding objects, and areas with important fine-grained details; such complexities currently require a slow dense scan [1, 2, 3, 4, 5, 6, 7, 8] to effectively reconstruct the 3D scene. However, in many of these scenarios, acquiring the 3D scene in the shortest time possible is often critical, e.g. for search and rescue, time is of essence, while for monitoring large construction or agricultural sites, battery life is often limiting. This often led researchers to develop techniques that are able to more judiciously scan a novel environment for resource-efficient 3D reconstruction, where resource constraints can be expressed as the number of acquisitions, distance traversed, acquisition time, or battery life. This problem has often been called the Next Best View (NBV) selection problem, where the goal is to predict a set of optimal camera viewpoints that can maximize reconstruction quality.

Predicting NBVs is a challenging problem due to the large search space for selecting the pose of each view, the challenge in efficiently computing the optimal solution in this non-convex space, and the complexity of scene geometry and occlusions. Earlier works on NBV often assume prior knowledge of the scene (e.g., a preliminary scan or CAD model) [9, 10, 11, 12, 13, 14], which limits applications in previously unexplored environments. Approaches that do not require prior knowledge of the scene predict NBVs by either maximizing coverage in the scene [15, 16, 17, 18, 19, 20] or by maximizing information gain [21, 11, 22] in the image space. While earlier methods have relied on heuristics or optimization [15, 16], recent methods often train a deep reinforcement learning (RL) algorithm [17, 18, 21, 11, 23, 22, 24, 25] to maximize coverage.

While maximizing coverage with RL [25, 18] may lead to a generalizable policy that can provide a good approximation of the scene, it ignores the fact that certain regions in a scene have more complicated geometry and self-occlusion than others. This means certain regions in the scene might require more captures than other regions to generate higher-quality reconstruction. For example, if the fence of the house occludes a part of the wall, a single viewpoint capture may satisfy the coverage criterion, but will lead to poor reconstruction with holes in the wall unless additional viewpoints are captured. Thus, our key idea is to develop an NBV acquisition policy that is trained to directly maximize the 3D reconstruction accuracy instead of only relying on the coverage criterion. We assume no prior information about the scene, and that the robot is equipped with an RGBD camera.

Our key idea is to formulate a greedy sequential next best view selection strategy, where at each step, we only capture a single ‘best’ next view that maximizes reconstruction improvement over the already captured set of base images. We repeat the process until some termination criterion has been reached. We achieve this by designing a View Introspection Network (VIN) that has been trained to assess the effectiveness of any query viewpoint in reducing reconstruction error over the observed base acquisitions. At each step of the acquisition, we uniformly sample query views around the object, evaluate their effectiveness by using the VIN, and choose the one that will maximize reconstruction improvement over the base views. We observe the greedy imitation learning approach of VIN-NBV to be more stable and effective than non-greedy RL based approaches.

Our key contribution is to design a lightweight neural network, VIN, that uses smart 3D-aware featurization to assess the effectiveness of any query viewpoint in reducing reconstruction error over an already captured set of views. We train VIN on simulated data using imitation learning, where we first calculate the true fitness score of the query view using relative reconstruction improvement over the base views. Our proposed VIN-NBV policy is generalizable and can operate under any kind of motion planning constraints and budget.

Experimental evaluation of the VIN-NBV policy with constraints on the number of acquisitions and time in motion indicate significant improvements of up to $\sim 30\%$ over a coverage only baseline, especially during earlier stages of acquisition. Ultimately both methods converge to the same solution under a very large time or acquisition budget.

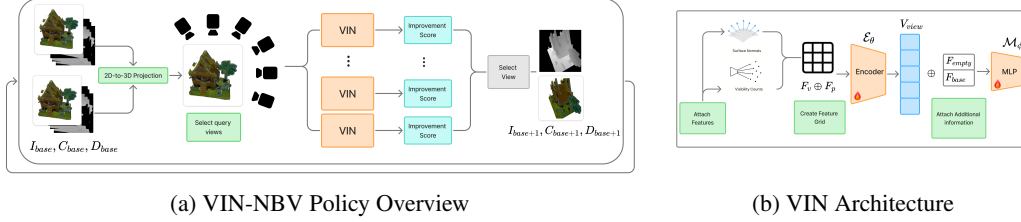


Figure 2: (a) VIN-NBV reconstructs the 3D scene from prior RGB-D captures, samples candidate viewpoints, and selects the one with the highest fitness predicted by the View Introspection Network (VIN) as the Next Best View (NBV), repeating until termination. (b) VIN uses a 3D-aware featurization, including surface normals, visibility count, and coverage (F_{empty}), and is trained via imitation learning to predict fitness as the Relative Reconstruction Improvement over current observations.

We also observe that VIN-NBV significantly outperforms existing RL-based algorithms that aim to maximize coverage. VIN-NBV reduces reconstruction error by 41% compared to Scan-RL [26] 39% compared to GenNBV [25].

2 Related work

NBV methods that require prior knowledge. Many existing approaches assume prior knowledge of the 3D scene, which limits applications in previously unexplored environments. Some approaches [9, 10, 11] directly exploit a pre-existing 3D model or its approximation. Some others rely on 2D maps, such as estimating the height of buildings as a rough 3D model [27] or obtaining a 2.5D model of the scene [14]. For scenes lacking pre-existing information, often a drone fly-through along a default trajectory is made to obtain an initial coarse reconstruction [16, 21]. In contrast, our method does not require any prior information about the scene and starts by acquiring two adjacent views and sequentially chooses the best next views until a specific termination criterion is met.

Optimal view selection from pre-capture imagery. Another line of work focuses on selecting an optimal subset of images from densely captured imagery to improve reconstruction quality. While earlier versions of these algorithms focused on selecting optimal views for Multiview Stereo Reconstruction [28, 1], more recent versions explored view selection for Neural Radiance Field (NeRF) and its variants [29, 30, 31, 22]. Our work is fundamentally different from this line of work, as we do not pre-capture the scene densely; rather, we only acquire images from the optimal viewpoints predicted by the NBV policy.

Criterion for predicting NBV. Previous approaches use proxy metrics like coverage [15, 18, 32, 17, 25] or information gain [33, 34, 35, 36] for predicting NBVs. State-of-the-art NBV techniques, GenNBV [25] and ScanRL [18], use Reinforcement Learning (RL) with coverage-based reward functions. While coverage-based policies may lead to reasonable reconstruction quality, they fail to account for complex structures and occlusions, often resulting in holes in the reconstructed scene. On the other hand, the information gain criterion is image-based and often lacks 3D knowledge of the scene, restricting generalization. Our work goes beyond coverage by directly maximizing the reconstruction quality, which leads to significant improvement under resource constraints, as shown empirically. Rather than relying on RL [18, 25], we design a greedy sequential policy, VIN-NBV, trained with imitation learning to help predict the reconstruction improvement of next views.

3 Method

We will first provide a mathematical overview of the NBV problem in Sec. 3.1. Then, we will introduce our proposed sampling-based greedy NBV policy, VIN-NBV, in Sec. 3.2, followed by the design of the View Introspection Network (VIN) in 3.3 and its training in 3.4.

3.1 Problem Setup

We consider a robot that has acquired k initial base images of a scene $I_{base} = \{I_1, \dots, I_k\}$ from viewpoints with camera parameters $C_{base} = \{C_1, \dots, C_k\}$ and depth maps $D_{base} = \{D_1, \dots, D_k\}$

either captured with a depth sensor or predicted with a Monocular Depth Estimator or Multi-View Stereo algorithms. The robot then runs a 3D reconstruction pipeline using the initial base views to reconstruct the 3D scene as \mathcal{R}_{base} . The goal of NBV is to predict a set of m next best views $C_{nbv} = \{C_1, \dots, C_m\}$ from which the scene should be captured to maximize the reconstruction quality of the scene.

More specifically, from C_{nbv} we capture NBV images $I_{nbv} = \{I_1, \dots, I_m\}$ and associated depth maps $D_{nbv} = \{D_1, \dots, D_m\}$ and perform 3D reconstruction to create \mathcal{R}_{final} using $I_{base} \cup I_{nbv}$ and $D_{base} \cup D_{nbv}$. While previous NBV techniques maximize coverage, we maximize reconstruction quality measured by the relative improvement of the chamfer distance of \mathcal{R}_{final} over \mathcal{R}_{base} :

$$C_{nbv}^* = \arg \max_{C_{nbv}} \frac{|CD(\mathcal{R}_{final}, \mathcal{R}_{GT}) - CD(\mathcal{R}_{base}, \mathcal{R}_{GT})|}{CD(\mathcal{R}_{base}, \mathcal{R}_{GT})}, \quad (1)$$

where $CD(\mathcal{R}, \mathcal{R}_{GT})$ calculates the chamfer distance between the reconstructed point cloud of scene \mathcal{R} and the ground-truth point cloud \mathcal{R}_{GT} .

3.2 NBV Policy with View Introspection Network

We propose a simple greedy imitation learning based approach, where for each acquisition, the robot samples a set of query camera viewpoints and evaluates their fitness, and chooses the ‘best’ one and repeats the process until some termination criterion has been reached. This acquisition policy has been described in Algorithm 1.

The VIN-NBV policy begins with I_{base}^k , C_{base}^k , D_{base}^k then iteratively selects next views until we have reached a desired termination criteria defined to fit downstream task constraints, e.g., number of image acquisitions, time traversed, battery life, etc. During each step, we create the most recent version of our reconstruction R_{base}^t by back-projecting our RGBD capture into 3D space. If RGB capture is made, 3D reconstruction techniques like Multiview Stereo or Monocular Depth Estimation can be used to reconstruct R_{base}^t . We then sample n query views around this reconstruction to evaluate their fitness and choose the ‘best’.

Algorithm 1 VIN-NBV Policy

```

1:  $I_{base}^k \leftarrow \{I_1, \dots, I_k\}$ 
2:  $C_{base}^k \leftarrow \{C_1, \dots, C_k\}$ 
3:  $D_{base}^k \leftarrow \{D_1, \dots, D_k\}$ 
4:  $t = k$ 
5: while not termination_criteria() do
6:   Reconstruct  $R_{base}^t$  from
   ( $I_{base}^t, C_{base}^t, D_{base}^t$ )
7:   Sample a set of query views  $\{q_i\}$ 
8:   for  $i = 1, \dots, n$  do
9:      $\widehat{\mathcal{RR}}\mathcal{I}(q_i) = \text{VIN}_\theta(R_{base}^t, C_{base}^t, C_{q_i})$ 
10:  end for
11:   $C_*^t \leftarrow \arg \max_q \mathcal{RR}\mathcal{I}(q)$ 
12:  Capture (or render)  $I_*^t$  and  $D_*^t$  from  $C_*^t$ 
13:   $I_{base}^{t+1} \leftarrow I_{base}^t \cup I_*^t$ 
14:   $D_{base}^{t+1} \leftarrow D_{base}^t \cup D_*^t$ 
15:   $C_{base}^{t+1} \leftarrow C_{base}^t \cup C_*^t$ 
16:   $t += 1$ 
17: end while
18: return  $R_{final}$ 

```

Our key idea is the introduction of the View Introspection Network (VIN), which independently evaluates potential query/next views and predicts their fitness. Instead of evaluating the fitness of each view to maximize coverage, we focus on maximizing the reconstruction quality. More specifically, we define fitness criterion as the Relative Reconstruction Improvement (\mathcal{RRI}) over the base views by capturing the query view q as defined in eq. 2. Relative Improvement is formulated to be independent of object types and scales, which otherwise affects the Chamfer Distance computation.

$$\mathcal{RRI}(q_i) = \frac{|CD(\mathcal{R}_{base \cup q_i}, \mathcal{R}_{GT}) - CD(\mathcal{R}_{base}, \mathcal{R}_{GT})|}{CD(\mathcal{R}_{base}, \mathcal{R}_{GT})}. \quad (2)$$

We train VIN to predict RRI fitness criterion $\widehat{\mathcal{RRI}}(q)$ for a query view q by taking the existing reconstruction R_{base} , camera parameters C_{base} , and query view camera parameters C_q as input:

$$\widehat{\mathcal{RRI}}(q) = \text{VIN}_\theta(R_{base}, C_{base}, C_q). \quad (3)$$

The design of VIN’s neural architecture and its training are described in Sec 3.3 and 3.4. After evaluating all n query views, VIN-NBV greedily selects the one with the highest improvement score. We move to the selected view position C_*^t and acquire new RGB-D capture which we use to update $I_{base}^t C_{base}^t D_{base}^t$ to get $I_{base}^{t+1} C_{base}^{t+1} D_{base}^{t+1}$. Once we have reached our desired stopping criteria, we create and return our final 3D reconstruction R_{final} using $I_{base}^m C_{base}^m D_{base}^m$.

Although we choose to use a simple greedy acquisition strategy, our policy provides the flexibility to use incorporate any desired constraints into the robots’ acquisition strategy. In Section 4, we evaluate VIN-NBV with constraints on the number of acquisitions and time in motion for the robot. Our method also allows the user to specify any specific sampling strategy to create a set of query views to evaluate, providing high adaptability to downstream applications.

3.3 Design of VIN

The VIN works by reconstructing the scene as a 3D point cloud from the base RGB-D capture \mathcal{R}_{base} , alternate techniques like Multiview Stereo can be used in the absence of a depth sensor. We attach simple lightweight features to every point in the point cloud by computing surface normals and the number of views in I_{base} in which each point is visible. Surface normal variance from later down-sampling provides helpful information about the local geometry of the scene. Higher variance can indicate regions of complex geometry that may need additional capture, and lower variance can indicate flatter areas where less capture is sufficient. Point visibility can serve as a confidence measure, where a query view with a high number of points visible in many prior captures is likely less helpful than views where points have a lower visibility.

We create a feature grid for each query view by projecting the featurized 3D point cloud \mathcal{R}_{base} into all n query cameras C_q . If a pixel on the feature grid does not map back to a point in the reconstructed point cloud, we simply assign a vector with all zeros, otherwise, we use the point features and depth after projection. Per-pixel depth values can help identify depth inconsistencies in the views, which may indicate gaps or holes in the reconstruction. Thus, for every query view, we obtain a feature grid of size $512 \times 512 \times 5$. We then downsample these feature grids using a pooling operation to obtain a 256×256 feature map F_p for each view. Down-sampling provides an explicit measure of local feature variance and helps reduce overall computation. We concatenate the per-pixel feature variances F_v with the feature map F_p to provide additional context about local geometric complexity.

We define a convolutional encoder $V_{view} = \mathcal{E}_\theta(F_v \oplus F_p)$ that is applied to the feature grids to transform the local per-pixel information into a global view feature vector V_{view} of size 256×1 , \oplus means concatenation. In addition to V_{view} , we also compute an empty feature F_{empty} to provide explicit information about reconstruction coverage, allowing the VIN to focus on learning key information on top of this to predict reconstruction improvement. Here, we consider a view pixel to be "empty" if it does not map back to a point in the reconstruction. To construct F_{empty} , we create a hull around the non-empty pixels in our query view and compute the number of empty pixels inside and outside of this hull. Empty pixels inside the hull expose "holes" in the existing reconstruction and can help measure how incomplete the currently captured geometry is. Empty pixels outside the hull correspond to image areas where no part of the current reconstruction is visible. Their count estimates the portion of the view that could reveal entirely new geometry. We concatenate both of these values to create the two-element F_{empty} feature vector. We use F_{empty} as a lightweight proxy for more traditional reconstruction coverage measures.

We also provide the number of base views F_{base} to help indicate at what stage in the capture we are at, since helpful views in the earlier stages look different from helpful views in later stages, and this may change how the model scores different views. We concatenate all of this information with V_{view} and pass it through a MLP $\mathcal{M}(\cdot)$ to predict the final improvement score:

$$\widehat{\mathcal{RRI}}(q) = \mathcal{M}_\phi(\mathcal{E}_\theta(F_v \oplus F_p) \oplus F_{empty} \oplus F_{base}). \quad (4)$$

3.4 Training of VIN

Our objective is to train the VIN to estimate the fitness of a query view, defined as its Relative Reconstruction Improvement ($\mathcal{RRI}(q)$) over the existing base views (as described in Equation 2). To achieve this, we adopt an imitation learning approach. At each acquisition step, we exhaustively compute the \mathcal{RRI} for a set of candidate query views by rendering their RGB-D images and reconstructing the point cloud using the new image along with the previously captured base images. This computed score, which relies on access to the ground-truth 3D model and rendering engine, is referred to as the Oracle RRI. VIN is then trained to predict this Oracle RRI, without access to the rendered image, using only the RGB-D images from previously captured views and the camera parameters of the query view.

However, directly regressing the \mathcal{RRI} proves to be challenging. The model struggles to generalize well across unseen objects and categories. To address this, we reformulate the task as a classification problem by discretizing the \mathcal{RRI} into 15 ordinal classes, where class 0 indicates the least improvement and class 14 the highest. In this formulation, we recognize that misclassifications between distant classes are more detrimental than those between nearby ones. Therefore, even if VIN cannot always predict the optimal next-best view, it should still identify a reasonably good one. To enforce this, we use a ranking-aware classification loss—CORAL [37]. CORAL transforms ordinal labels into a series of binary classification tasks, encouraging predictions that respect the natural order of the labels. This improves model predictions and reduces large misclassification errors.

An additional challenge arises in defining consistent class labels across different stages of acquisition. Early acquisitions often have higher \mathcal{RRI} values because large portions of the scene remain unseen, so view selection has a greater impact. In contrast, later stages typically yield lower \mathcal{RRI} values, as improvements become more incremental, focusing on resolving occlusions and small gaps. Using a fixed class assignment strategy across all stages would misclassify even the best views in later stages into lower-quality categories.

To overcome this, we normalize \mathcal{RRI} values in a stage-independent manner. We group our training data by capture stage, defined by the number of base views, and determine the standard deviation and mean of the \mathcal{RRI} values in these groups. We then take \mathcal{RRI} for each query view and convert it into a z-score based on the number of standard deviations they are from the mean of their group. We soft clip the z-scores using a tanh function, to prevent extreme outliers, and then group views into 15 dynamically sized bins, ensuring a similar number of samples in each bin. We use these bins as our final class labels.

3.5 Implementation Details

Model Implementation. We implement our model using Pytorch [38] and conduct training using Pytorch Lightning [39]. We leverage Pytorch3D[40] to help create, and render our point clouds. Our convolutional encoder has 4 layers and hidden dimension size of 256. Our rank MLP has 3 layers with a hidden dimension size of 256 and uses a CORAL [37] layer as its final layer so that we can use the CORAL loss during training. We use the open-source implementation of this loss and other necessary components provided by the authors on [GitHub](#).

Point Cloud Projection. To project our point clouds to query views, we use the Pytorch3D[40] PointsRasterizer with a points per pixel setting of 1 and a fixed radius of 0.01. Since the rasterizer uses a normalized coordinate system and our voxel down sampling leads to evenly spaced points we find that this fixed radius size is sufficient. During the projection process for the point cloud we save a mapping from pixel to point allowing us to determine per pixel feature vectors to construct a feature grid. We do all projection in batch.

Model Training. We train our model for 60 epochs using the AdamW[41] optimizer and a cosine annealing[42] learning rate scheduler. For our learning rate we used 1e-3 and train for approximately 24 hours on four A6000 GPUs. During training time we treat each set of next views for one specific object as a single batch. Batching by object means we only need to reconstruct one point cloud for an entire batch and can project it to all candidate views in one go, saving memory and computation.

Evaluation Data Preparation. The authors of GenNBV [25] resized the house objects from OmniObject3D [43] to better fit their problem context. The resized objects were made available by the authors on the project GitHub and we used them to calculate the exact scale factor applied to the original OmniObject3D [43] houses. We use this scale factor to bring our chamfer distance values computed on the unscaled objects into the correct scale for direct comparison.

4 Experiments

We evaluate the effectiveness of VIN-NBV and compare it to existing NBV approaches to select viewpoints enabling high-quality 3D reconstructions on standard datasets. We specifically focus on scenarios where a robot can acquire only a few images or its motion time is limited.

Datasets. We follow the same train-test protocol from GenNBV[25] by training on a modified subset of Houses3K [18], and testing on the house category from OmniObject3D [43]. We also evaluate our method on additional classes (see Section 4.3). We begin the acquisition process by selecting two base views from 120 renders of the object. The first base view is randomly selected, and the second one is the view with the closest camera position to the first.

Baselines. We compare our VIN-NBV policy against several existing 3D-based next-best-view (NBV) approaches, including ScanRL [18], GenNBV [25], and ActiveRMap [44]. Since the evaluation code and model weights of GenNBV[25] are unavailable, we did our best to reproduce their evaluation framework to directly compare with their reported results in the paper. We also perform a direct visual comparison to the reconstruction results provided in their paper, as seen in Fig. 3. Additionally, we include two baseline methods: Coverage NBV and Oracle NBV.

Coverage NBV shares the same greedy view selection strategy as VIN-NBV, but instead of using VIN’s predicted \mathcal{RRL} score (line 9 in Algorithm 1), it relies on a coverage-based fitness function, $Cov(q) = W \times H - \sum_{u=1}^H \sum_{v=1}^W \mathbb{1}(C_q(\mathcal{R}_{base})_{u,v})$, where $W \times H$ is the image resolution and $\mathbb{1}(\cdot)$ is an indicator function. This function estimates the number of empty pixels in the query view C_q when rendering the current reconstructed 3D point cloud \mathcal{R}_{base} . A higher $Cov(q)$ score suggests that the query view covers more previously unseen areas, making it a potentially valuable viewpoint.

Similarly, the Oracle NBV baseline is a variant of the VIN-NBV policy, where the fitness function (line 9 in Algorithm 1) is replaced with the ground-truth Relative Reconstruction Improvement (\mathcal{RRL}) of each query view. This method assumes access to the complete ground-truth reconstruction, enabling direct computation of \mathcal{RRL} as defined in Equation 2.

For all sampling-based acquisition policies, VIN-NBV, Cov-NBV, and Oracle-NBV, we uniformly render 120 viewpoints in 3 hemispherical shells around the object from which the policies can sample during evaluation.

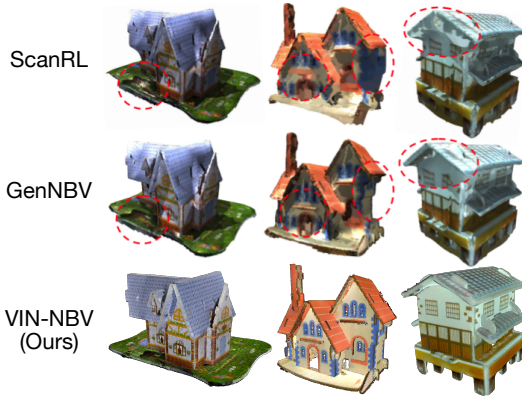


Figure 3: We compare reconstruction quality of our VIN-NBV policy with GenNBV [25] and ScanRL [18] on 3 objects using 20 captures and a modified version of the figure also depicted in the original GenNBV [25] paper.

OmniObject3D	
NBV Policy	Accuracy (cm) ↓
Random Hemisphere	0.48
Uniform Hemisphere	0.41
Uncertainty-Guided	0.41
ActiveRMap, Arxiv’22[44]	0.38
Scan-RL, ECCV’20[18]	0.37
GenNBV, CVPR’24[25]	0.33
VIN-NBV (Ours)	0.20

Table 1: Quantitative evaluation of NBV policies on OmniObject3D [43] houses (20 acquisitions) using chamfer distance. We follow the evaluation setup of GenNBV and report the performance of existing methods from their paper.

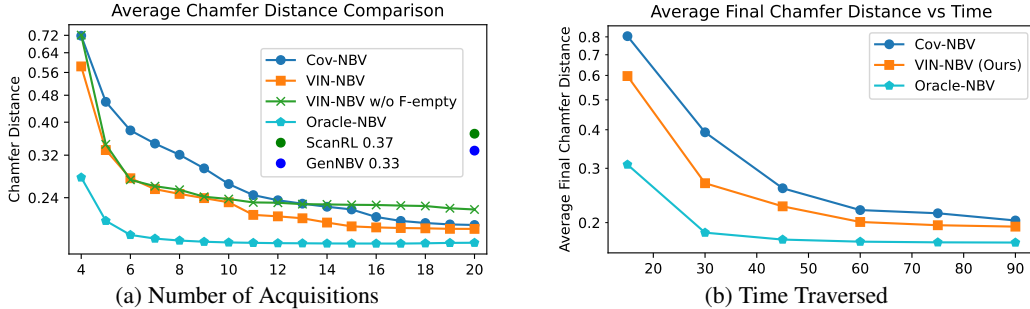


Figure 4: Quantitative evaluation of NBV policies on OmniObject3D [43], showing average reconstruction error (in cm) under constraints on (a) number of acquisitions and (b) time traversed.

Metrics. Since our goal is to improve reconstruction quality, we use chamfer distance as our main accuracy metric, as it can capture fine-grained information at the point level. For each object, we calculate the chamfer distance between the reconstructed and the ground truth point clouds. We report the average accuracy (chamfer distance) in centimeters across all objects in Omniobject3D houses [43].

4.1 Evaluation with Limited Number of Acquisitions

To enable direct comparison with GenNBV and ScanRL [45, 18], we evaluate our policy on the OmniObject3D [43] houses dataset, limited to 20 captures. VIN-NBV outperforms state-of-the-art NBV policies (Table 1), achieving an average reconstruction error of 0.20 cm on houses, compared to 0.33 cm for GenNBV [25] and 0.37 cm for ScanRL. A visual comparison is presented in Fig. 3, modified directly from the visuals presented in the GenNBV [25] paper, shows VIN-NBV retains finer detail, whereas GenNBV and ScanRL produce blurrier results despite good coverage.

In Figure. 4a we compare the reconstruction accuracy during the intermediate stages of acquisition between VIN-NBV with the coverage baseline ‘Cov-NBV’ and the ‘Oracle NBV’. We observe that large improvements with respect to the coverage baseline are observed during the initial stages of capture, while towards the later stages, both policies result in similar reconstruction quality. Since the model weights and the evaluation code of the GenNBV [25] paper are unavailable, we were unable to evaluate this method during the intermediate stages of the capture process.

Ablation: Importance of coverage feature F_{empty} in VIN. To understand the importance of the coverage feature we provide with F_{empty} , we run an ablation that evaluates the VIN-NBV policy using a VIN model trained without this information. In Fig. 4a, we see that the absence of coverage features makes no difference during earlier acquisition stages but makes a substantial difference during the later stages. This explains why VIN-NBV achieves large gains over Cov-NBV early on, converging to a similar solution during later stages where coverage is helpful. Although VIN focuses on predicting reconstruction quality, the coverage feature is still a helpful indicator, which is otherwise hard to learn implicitly during training.

4.2 Evaluation with Time-Limited Robot Motion

In our time-limited setting, we evaluate our policy under varying constraints on time in motion to understand its efficiency under strict budgets, simulating many critical time-sensitive applications. We assume that the robot is a drone equipped with a depth sensor and camera and travels at a constant velocity of 4 mph, a typical speed for consumer-grade drones. We assume that the drone always takes a straight-line path to the next capture position and determine how far it can travel under different time limits. We use the same OmniObject3D [43] evaluation data as before and scaled all objects to a size of 14 meters to simulate a more realistic capture setting.

Adapting NBV policies for time-limited acquisitions. At each step during capture, our robot checks how far it can still travel and finds all potential next views that are within range. If our robot is not able to find a next view within range, it stops capture and computes the chamfer distance of

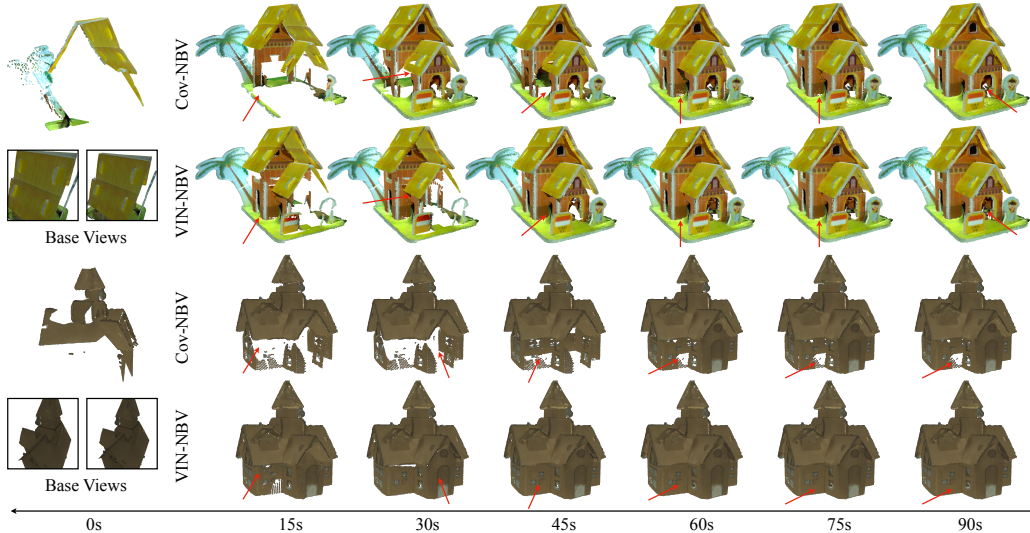


Figure 5: We visualize reconstruction obtained by VIN-NBV and Cov-NBV for different constraints on time traversed. For smaller time budgets, VIN-NBV reconstructions are better with fewer holes.

the reconstruction with the current captures. We use our VIN-NBV policy to select the next views and do not impose a limit on the number of images that the robot can capture in this setting.

We show our results from the time-limited setting in Fig. 4b. Under all time constraints, our method outperforms the coverage baseline, with the largest improvement happening under the strictest time constraints. During the 15 second time limit our method outperforms the coverage baseline by $\sim 25\%$. In Figure. 5, we visualize the reconstructed 3D scene using our VIN-NBV policy and the coverage baseline (Cov-NBV) for varying time constraints, illustrating that with more available time, the policy focuses on capturing views that can fill missing regions and holes in the reconstruction.

4.3 Generalization Across Object Categories

We evaluate our policy on additional object categories from OmniObject3D [43], namely dinosaurs, toy animals, and toy motorcycles. Many of the house objects contain largely planar surfaces with large flat regions and overall less curvature and self-occlusion, in contrast the additional object classes we evaluated have much more detailed surface geometry and instances of self-occlusion. Our results show that even with these new complexities our policy is able to generalize well.

In Fig.6 we see that when we evaluate our VIN-NBV policy on additional object categories, our policy is able to consistently outperform the coverage baseline. Larger gaps in performance occur early on, with both methods reaching similar final chamfer distance values at 20 captures. Our policy does particularly well, compared to the coverage baseline, for objects with more complex self-occlusions such as the toy motorcycle class. We include visual results of our policy and the coverage baseline after 10 acquisitions on several objects and from various viewing angles in Fig.8, Fig.10, Fig.9, Fig.11.

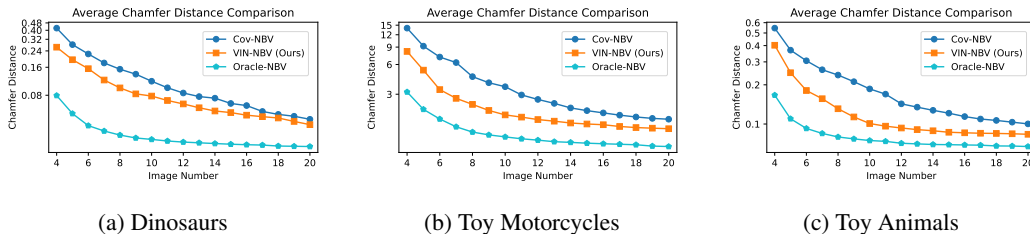


Figure 6: We graph the average chamfer distance at each capture stage in three additional object classes namely dinosaurs, toy motorcycles, and toy animals. We compare VIN-NBV to a coverage baseline for 20 captures.

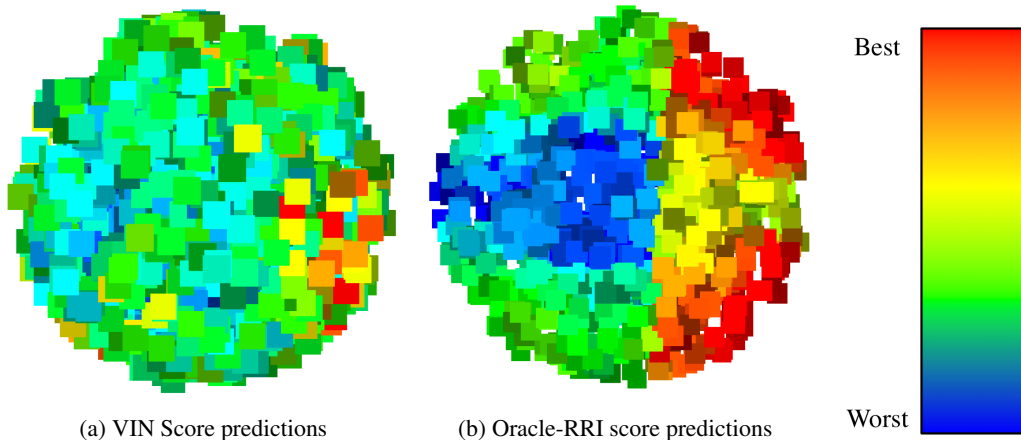


Figure 7: 3D heatmap (top-down view) indicating the fitness score predicted by (a) our VIN policy and (b) the Oracle-NBV during the first capture step on house 1 from OmniObject3D [43]. Each point marks a query-view camera position, colored by its predicted reconstruction improvement score (blue=low, red=high). While VIN-NBV has high precision, accurately identifying the most helpful viewpoints, it has low recall, often missing many useful views.

5 Limitations

RGB-D vs RGB capture. We use ground truth depth maps in RGB-D capture to match the evaluation setting of the prior works GenNBV [25] and ScanRL [26], but these depth maps are noise-free and not reflective of true depth sensor readings. We observe that depth maps estimated from RGB images using Monocular Depth Estimation [46, 47] often lack multiview consistency and struggle with handling the scale of different objects especially with our synthetic data. Depth maps from MultiView Stereo algorithms [48, 49] often require more than 3 views and perform poorly with just 2 base images. Since VIN relies on 3D-aware featurization, inaccurate and multiview inconsistent depth maps can lead to a poorly reconstructed 3D scene and featurization, which the VIN network struggles to handle.

Performance gap with Oracle-NBV. Our method shows a significant gap to our Oracle-NBV baseline in the early capture stages, indicating that there is still room for improvement. In Fig. 4a we see that the Oracle baseline is able to make significantly better choices early on and converge much faster than our policy. In Fig. 4b, we see that even with less time, the oracle baseline is still able to outperform our policy, and as more time is added, it converges much sooner. These gaps may indicate that the VIN is unable to properly mimic the behavior of the Oracle-NBV.

To understand this, in Fig. 7, we make a simple visualization of the 3D heatmap of Relative Reconstruction Improvement scores of densely sampled query views around the object, calculated by the VIN-NBV and the Oracle-NBV, for the first capture step of house 1 from OmniObject3D. We observe that while Oracle-NBV calculates a relatively large set of query views to be effective with high fitness scores (marked in red), VIN-NBV only predicts a subset of these views to be effective, and misses out on a large set of potentially good views. Hence, during evaluation, the chances of VIN-NBV finding a ‘good’ view from a small set of sampled views is low, and can explain the performance gap between Oracle-NBV and VIN-NBV.

6 Conclusion

In this paper, we revisited the Next Best View problem and proposed the VIN and VIN-NBV policy, a generalizable policy that can determine a set of optimal acquisitions to maximize reconstruction quality. Our policy can be easily adapted to operate with limitations on the number of acquisitions or a time limit on robot motion. By optimizing for reconstruction quality rather than traditional coverage, VIN-NBV improves final reconstruction results without requiring prior scene knowledge, extra image captures, per-scene training, or complex RL policies. Evaluations on OmniObject3D

[43] show VIN-NBV outperforms state-of-the-art RL methods, reducing reconstruction error by up to 40%. VIN-NBV can enable robots to efficiently acquire necessary 3D information for various applications where time is of the essence.

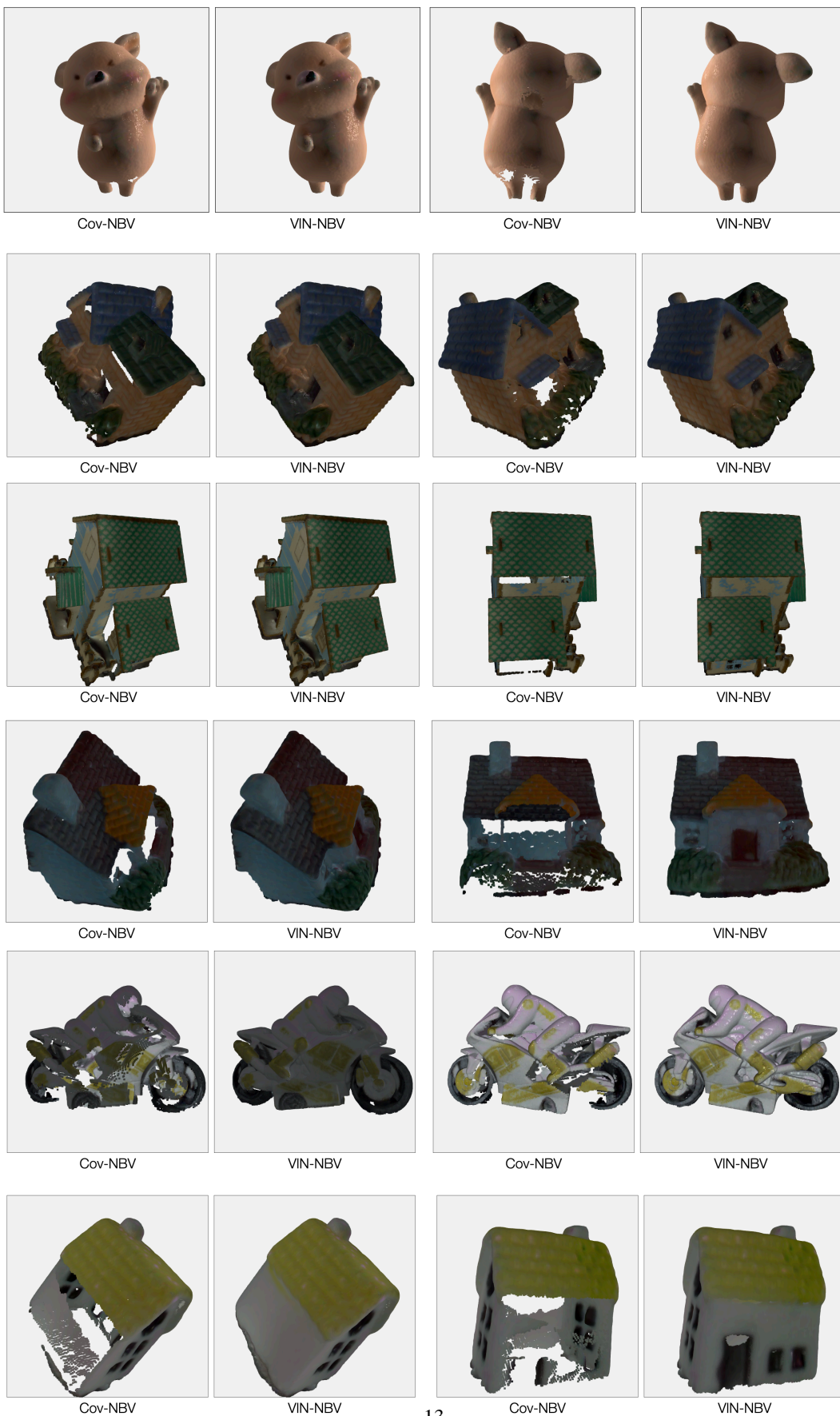
View 1

View 2



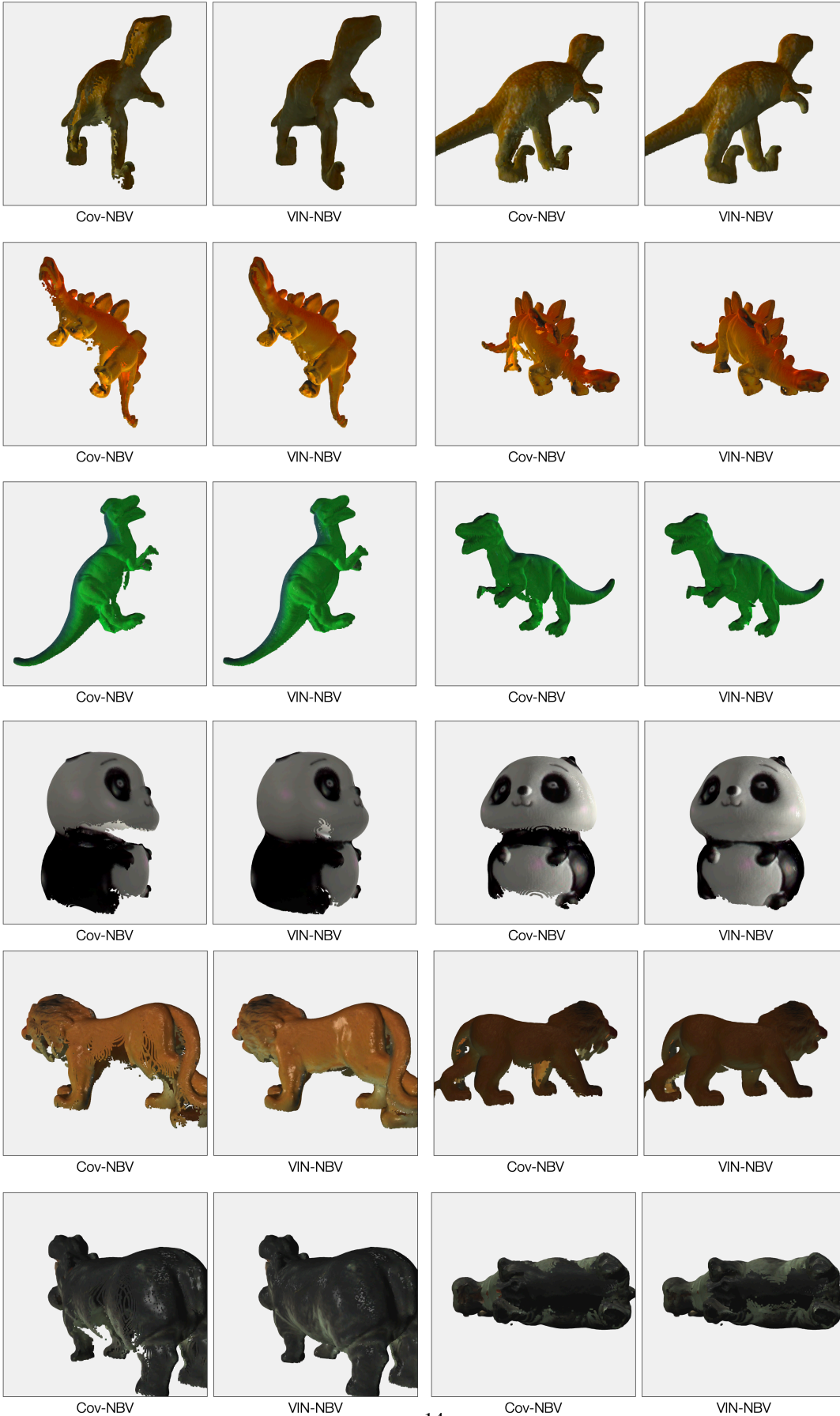
View 1

View 2



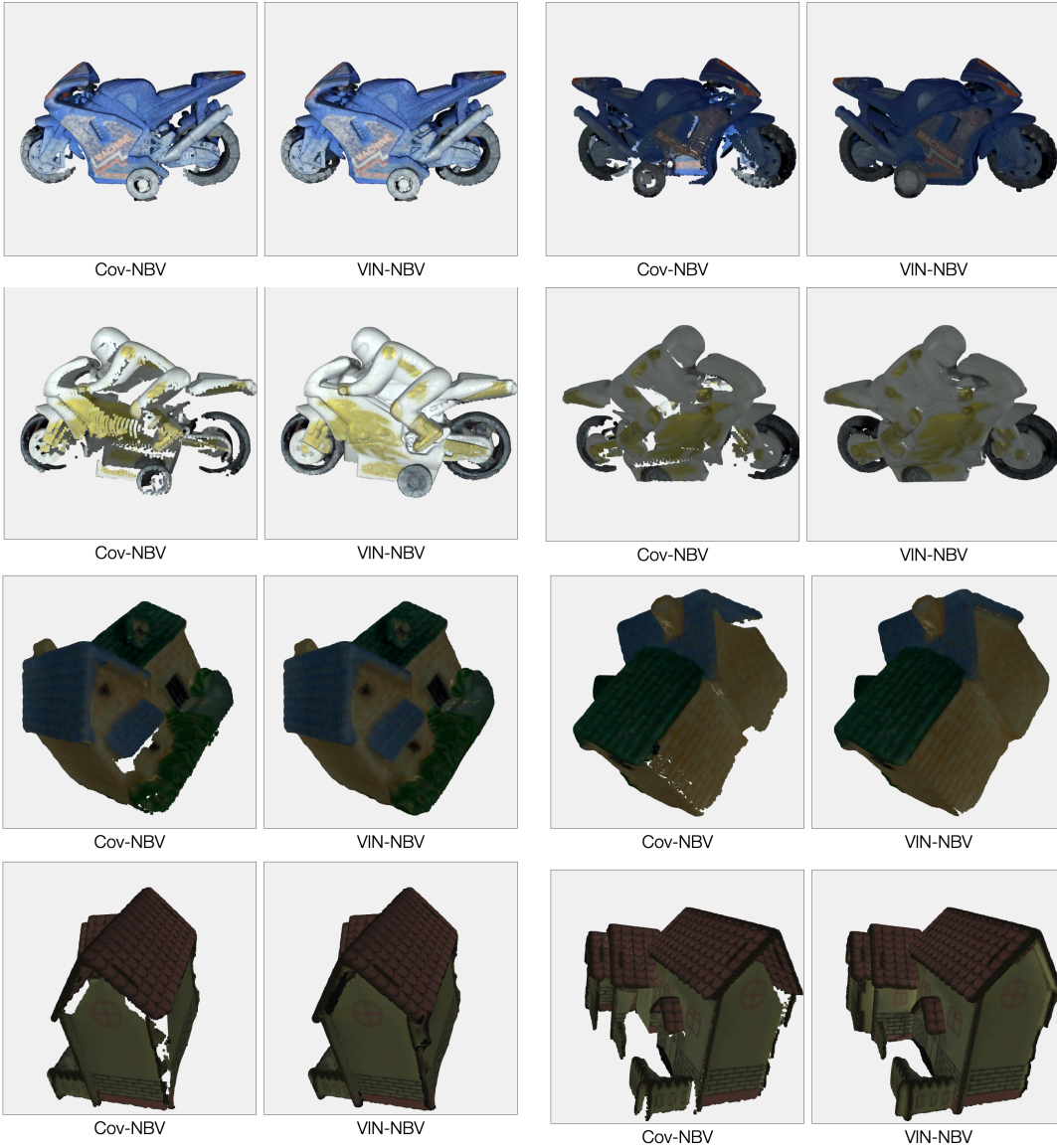
View 1

View 2



View 1

View 2



References

- [1] Y. Furukawa, B. Curless, S. M. Seitz, and R. Szeliski. Towards internet-scale multi-view stereo. In *2010 IEEE computer society conference on computer vision and pattern recognition*, pages 1434–1441. IEEE, 2010.
- [2] J. L. Schönberger, E. Zheng, J.-M. Frahm, and M. Pollefeys. Pixelwise view selection for unstructured multi-view stereo. In *Computer Vision–ECCV 2016: 14th European Conference, Amsterdam, The Netherlands, October 11-14, 2016, Proceedings, Part III 14*, pages 501–518. Springer, 2016.
- [3] J.-M. Frahm, P. Fite-Georgel, D. Gallup, T. Johnson, R. Raguram, C. Wu, Y.-H. Jen, E. Dunn, B. Clipp, S. Lazebnik, et al. Building rome on a cloudless day. In *Computer Vision–ECCV 2010: 11th European Conference on Computer Vision, Heraklion, Crete, Greece, September 5-11, 2010, Proceedings, Part IV 11*, pages 368–381. Springer, 2010.
- [4] S. Agarwal, Y. Furukawa, N. Snavely, I. Simon, B. Curless, S. M. Seitz, and R. Szeliski. Building rome in a day. *Communications of the ACM*, 54(10):105–112, 2011.
- [5] M. Bleyer, C. Rhemann, and C. Rother. Patchmatch stereo-stereo matching with slanted support windows. In *Bmvc*, volume 11, pages 1–11, 2011.
- [6] Y. Furukawa and J. Ponce. Accurate, dense, and robust multiview stereopsis. *IEEE transactions on pattern analysis and machine intelligence*, 32(8):1362–1376, 2009.
- [7] M. Goesele, N. Snavely, B. Curless, H. Hoppe, and S. M. Seitz. Multi-view stereo for community photo collections. In *2007 IEEE 11th international conference on computer vision*, pages 1–8. IEEE, 2007.
- [8] C. Strecha, R. Fransens, and L. Van Gool. Wide-baseline stereo from multiple views: a probabilistic account. In *Proceedings of the 2004 IEEE Computer Society Conference on Computer Vision and Pattern Recognition, 2004. CVPR 2004.*, volume 1, pages I–I. IEEE, 2004.
- [9] M. Devrim Kaba, M. Gokhan Uzunbas, and S. Nam Lim. A reinforcement learning approach to the view planning problem. In *Proceedings of the IEEE Conference on Computer Vision and Pattern Recognition*, pages 6933–6941, 2017.
- [10] Y. Sun, Q. Huang, D.-Y. Hsiao, L. Guan, and G. Hua. Learning view selection for 3d scenes. In *Proceedings of the IEEE/CVF Conference on Computer Vision and Pattern Recognition*, pages 14464–14473, 2021.
- [11] H. Zhang, Y. Yao, K. Xie, C.-W. Fu, H. Zhang, and H. Huang. Continuous aerial path planning for 3d urban scene reconstruction. *ACM Trans. Graph.*, 40(6):225–I, 2021.
- [12] F. Yan, E. Xia, Z. Li, and Z. Zhou. Sampling-based path planning for high-quality aerial 3d reconstruction of urban scenes. *Remote Sensing*, 13(5):989, 2021.
- [13] W. Jing, J. Polden, P. Y. Tao, W. Lin, and K. Shimada. View planning for 3d shape reconstruction of buildings with unmanned aerial vehicles. In *2016 14th International Conference on Control, Automation, Robotics and Vision (ICARCV)*, pages 1–6, 2016. doi: [10.1109/ICARCV.2016.7838774](https://doi.org/10.1109/ICARCV.2016.7838774).
- [14] X. Zhou, K. Xie, K. Huang, Y. Liu, Y. Zhou, M. Gong, and H. Huang. Offsite aerial path planning for efficient urban scene reconstruction. *ACM Transactions on Graphics (TOG)*, 39(6):1–16, 2020.
- [15] J. Maver and R. Bajcsy. Occlusions as a guide for planning the next view. *IEEE transactions on pattern analysis and machine intelligence*, 15(5):417–433, 1993.

- [16] M. Roberts, D. Dey, A. Truong, S. Sinha, S. Shah, A. Kapoor, P. Hanrahan, and N. Joshi. Submodular trajectory optimization for aerial 3d scanning. In *Proceedings of the IEEE International Conference on Computer Vision*, pages 5324–5333, 2017.
- [17] B. Hepp, D. Dey, S. N. Sinha, A. Kapoor, N. Joshi, and O. Hilliges. Learn-to-score: Efficient 3d scene exploration by predicting view utility. In *Proceedings of the European conference on computer vision (ECCV)*, pages 437–452, 2018.
- [18] D. Peralta, J. Casimiro, A. M. Nilles, J. A. Aguilar, R. Atienza, and R. Cajote. Next-best view policy for 3d reconstruction. In *Computer Vision–ECCV 2020 Workshops: Glasgow, UK, August 23–28, 2020, Proceedings, Part IV 16*, pages 558–573. Springer, 2020.
- [19] A. Guédon, P. Monasse, and V. Lepetit. Scone: Surface coverage optimization in unknown environments by volumetric integration. *Advances in Neural Information Processing Systems*, 35:20731–20743, 2022.
- [20] A. Guédon, T. Monnier, P. Monasse, and V. Lepetit. MACARONS: Mapping And Coverage Anticipation with RGB ONline Self-supervision. In *CVPR*, 2023.
- [21] B. Hepp, M. Nießner, and O. Hilliges. Plan3d: Viewpoint and trajectory optimization for aerial multi-view stereo reconstruction. *ACM Transactions on Graphics (TOG)*, 38(1):1–17, 2018.
- [22] W. Jiang, B. Lei, and K. Daniilidis. Fisherrf: Active view selection and uncertainty quantification for radiance fields using fisher information. *arXiv preprint arXiv:2311.17874*, 2023.
- [23] Y. Ran, J. Zeng, S. He, J. Chen, L. Li, Y. Chen, G. Lee, and Q. Ye. Neurar: Neural uncertainty for autonomous 3d reconstruction with implicit neural representations. *IEEE Robotics and Automation Letters*, 8(2):1125–1132, 2023.
- [24] R. Zeng, W. Zhao, and Y.-J. Liu. Pc-nbv: A point cloud based deep network for efficient next best view planning. In *2020 IEEE/RSJ International Conference on Intelligent Robots and Systems (IROS)*, pages 7050–7057, 2020. doi:10.1109/IROS45743.2020.9340916.
- [25] X. Chen, Q. Li, T. Wang, T. Xue, and J. Pang. Gennbv: Generalizable next-best-view policy for active 3d reconstruction. In *Proceedings of the IEEE/CVF Conference on Computer Vision and Pattern Recognition*, pages 16436–16445, 2024.
- [26] J. Schulman, F. Wolski, P. Dhariwal, A. Radford, and O. Klimov. Proximal policy optimization algorithms. *arXiv preprint arXiv:1707.06347*, 2017.
- [27] W. Jing, J. Polden, P. Y. Tao, W. Lin, and K. Shimada. View planning for 3d shape reconstruction of buildings with unmanned aerial vehicles. In *2016 14th International Conference on Control, Automation, Robotics and Vision (ICARCV)*, pages 1–6. IEEE, 2016.
- [28] A. Hornung, B. Zeng, and L. Kobbelt. Image selection for improved multi-view stereo. In *2008 IEEE Conference on Computer Vision and Pattern Recognition*, pages 1–8. IEEE, 2008.
- [29] E. J. Smith, M. Drozdal, D. Nowrouzezahrai, D. Meger, and A. Romero-Soriano. Uncertainty-driven active vision for implicit scene reconstruction. *arXiv preprint arXiv:2210.00978*, 2022.
- [30] X. Pan, Z. Lai, S. Song, and G. Huang. Activenerf: Learning where to see with uncertainty estimation. In *European Conference on Computer Vision*, pages 230–246. Springer, 2022.
- [31] K. Lee, S. Gupta, S. Kim, B. Makwana, C. Chen, and C. Feng. So-nerf: Active view planning for nerf using surrogate objectives. *arXiv preprint arXiv:2312.03266*, 2023.
- [32] Robot rescuers to help save lives after disasters. <https://ec.europa.eu/research-and-innovation/en/horizon-magazine/robot-rescuers-help-save-lives-after-disasters>. Written 19 March 2014.

- [33] S. Lee, L. Chen, J. Wang, A. Liniger, S. Kumar, and F. Yu. Uncertainty guided policy for active robotic 3d reconstruction using neural radiance fields, 2022. URL <https://arxiv.org/abs/2209.08409>.
- [34] S. Isler, R. Sabzevari, J. Delmerico, and D. Scaramuzza. An information gain formulation for active volumetric 3d reconstruction. In *2016 IEEE International Conference on Robotics and Automation (ICRA)*, pages 3477–3484, 2016. doi:10.1109/ICRA.2016.7487527.
- [35] C. Potthast and G. S. Sukhatme. A probabilistic framework for next best view estimation in a cluttered environment. *Journal of Visual Communication and Image Representation*, 25(1):148–164, 2014. ISSN 1047-3203. doi:<https://doi.org/10.1016/j.jvcir.2013.07.006>. URL <https://www.sciencedirect.com/science/article/pii/S1047320313001387>. Visual Understanding and Applications with RGB-D Cameras.
- [36] W. Jiang, B. Lei, and K. Daniilidis. Fisherrf: Active view selection and uncertainty quantification for radiance fields using fisher information, 2024. URL <https://arxiv.org/abs/2311.17874>.
- [37] W. Cao, V. Mirjalili, and S. Raschka. Rank consistent ordinal regression for neural networks with application to age estimation. *Pattern Recognition Letters*, 140:325–331, 2020. ISSN 0167-8655. doi:<https://doi.org/10.1016/j.patrec.2020.11.008>. URL <http://www.sciencedirect.com/science/article/pii/S016786552030413X>.
- [38] A. Paszke, S. Gross, F. Massa, A. Lerer, J. Bradbury, G. Chanan, T. Killeen, Z. Lin, N. Gimelshein, L. Antiga, A. Desmaison, A. Köpf, E. Yang, Z. DeVito, M. Raison, A. Tejani, S. Chilamkurthy, B. Steiner, L. Fang, J. Bai, and S. Chintala. Pytorch: An imperative style, high-performance deep learning library, 2019. URL <https://arxiv.org/abs/1912.01703>.
- [39] W. Falcon and The PyTorch Lightning team. PyTorch Lightning, Mar. 2019. URL <https://github.com/Lightning-AI/lightning>.
- [40] N. Ravi, J. Reizenstein, D. Novotny, T. Gordon, W.-Y. Lo, J. Johnson, and G. Gkioxari. Accelerating 3d deep learning with pytorch3d. *arXiv:2007.08501*, 2020.
- [41] I. Loshchilov and F. Hutter. Decoupled weight decay regularization, 2019. URL <https://arxiv.org/abs/1711.05101>.
- [42] I. Loshchilov and F. Hutter. Sgdr: Stochastic gradient descent with warm restarts, 2017. URL <https://arxiv.org/abs/1608.03983>.
- [43] T. Wu, J. Zhang, X. Fu, Y. Wang, J. Ren, L. Pan, W. Wu, L. Yang, J. Wang, C. Qian, et al. Omniobject3d: Large-vocabulary 3d object dataset for realistic perception, reconstruction and generation. In *Proceedings of the IEEE/CVF Conference on Computer Vision and Pattern Recognition*, pages 803–814, 2023.
- [44] H. Zhan, J. Zheng, Y. Xu, I. Reid, and H. Rezatofghi. Activermap: Radiance field for active mapping and planning, 2022. URL <https://arxiv.org/abs/2211.12656>.
- [45] L. Qi, J. Wu, S. Wang, and S. Sengupta. My3dgen: Building lightweight personalized 3d generative model. *arXiv preprint arXiv:2307.05468*, 2023.
- [46] B. Ke, A. Obukhov, S. Huang, N. Metzger, R. C. Daudt, and K. Schindler. Repurposing diffusion-based image generators for monocular depth estimation. In *Proceedings of the IEEE/CVF Conference on Computer Vision and Pattern Recognition (CVPR)*, 2024.
- [47] J. Wang, M. Chen, N. Karaev, A. Vedaldi, C. Rupprecht, and D. Novotny. Vggt: Visual geometry grounded transformer. In *Proceedings of the IEEE/CVF Conference on Computer Vision and Pattern Recognition*, 2025.

- [48] J. L. Schonberger and J.-M. Frahm. Structure-from-motion revisited. In *Proceedings of the IEEE conference on computer vision and pattern recognition*, pages 4104–4113, 2016.
- [49] C. Cao, X. Ren, and Y. Fu. Mvsformer++: Revealing the devil in transformer’s details for multi-view stereo. *arXiv preprint arXiv:2401.11673*, 2024.